Ion irradiation of the native oxide/silicon surface increases the thermal boundary conductance across aluminum/silicon interfaces

Caroline S. Gorham,[1] Khalid Hattar,[2] Ramez Cheaito,[1] John C. Duda,[1,*] John T. Gaskins,[1] Thomas E. Beechem,[2] Jon F. Ihlefeld,[2] Laura B. Biedermann,[2] Edward S. Piekos,[2] Douglas L. Medlin,[3] and Patrick E. Hopkins[1,†]

[1]*Department of Mechanical and Aerospace Engineering, University of Virginia, Charlottesville, Virginia 22904, USA*

[2]*Sandia National Laboratories, Albuquerque, New Mexico 87123, USA*

[3]*Sandia National Laboratories, Livermore, California 94550, USA*

(Received 9 February 2014; published 3 July 2014)

The thermal boundary conductance across solid-solid interfaces can be affected by the physical properties of the solid boundary. Atomic composition, disorder, and bonding between materials can result in large deviations in the phonon scattering mechanisms contributing to thermal boundary conductance. Theoretical and computational studies have suggested that the mixing of atoms around an interface can lead to an increase in thermal boundary conductance by creating a region with an average vibrational spectra of the two materials forming the interface. In this paper, we experimentally demonstrate that ion irradiation and subsequent modification of atoms at solid surfaces can increase the thermal boundary conductance across solid interfaces due to a change in the acoustic impedance of the surface. We measure the thermal boundary conductance between thin aluminum films and silicon substrates with native silicon dioxide layers that have been subjected to proton irradiation and post-irradiation surface cleaning procedures. The thermal boundary conductance across the Al/native oxide/Si interfacial region increases with an increase in proton dose. Supported with statistical simulations, we hypothesize that ion beam mixing of the native oxide and silicon substrate within ∼2.2 nm of the silicon surface results in the observed increase in thermal boundary conductance. This ion mixing leads to the spatial gradation of the silicon native oxide into the silicon substrate, which alters the acoustic impedance and vibrational characteristics at the interface of the aluminum film and native oxide/silicon substrate. We confirm this assertion with picosecond acoustic analyses. Our results demonstrate that under specific conditions, a "more disordered and defected" interfacial region can have a lower resistance than a more "perfect" interface.

DOI: 10.1103/PhysRevB.90.024301 PACS number(s): 66.70.Df, 63.22.−m, 68.35.Ja, 61.80.Jh

I. INTRODUCTION

The fundamental mechanisms driving phonon scattering at interfaces and boundaries have been the focus of an extremely active area of research over the past few decades [1–3], mainly driven by nanotechnology and thermal engineering of nanosystems [3,4]. In general, the phonon scattering mechanisms at boundaries and interfaces differ from those in homogeneous materials. Phonon-interface and boundary scattering has led to remarkable observations such as extremely low thermal conductivities of layered solids [5,6], functional group-modified thermal transport across interfaces in nanosystems [7–12], large thermoelectric figure of merit in nanowires [13,14], manipulation of phonon scattering in alloy-based nanosystems [15–18], and asymmetric heat conduction [19]. However, disorder or imperfections around interfaces can lead to further changes in thermal transport that are relatively not well understood [1]. In general, interfacial imperfections have been observed to lead to a decrease in phonon thermal boundary conductance [1]. We have experimentally observed this decrease in thermal boundary conductance across interfaces with roughness (i.e., geometric disorder) [20,21], an amorphous layer (i.e., structural disorder) [22–24], dislocations [25], and elemental mixing resulting in both compositional and structural disorder [26]. In each of these cases, the disorder led to a reduction in thermal boundary conductance.

However, theoretical and computational investigations have shown that with specific tailoring of this interfacial disorder or masses, an increase in thermal boundary conductance across solid interfaces could be realized through coupled phonon modes near an interface that effectively bridge the two phonon spectra. This concept is similar to that theorized by Huberman and Overhauser [27], who described heat transport across lead/diamond [28,29] interfaces as being enhanced by "joint modes." These joint modes, which originate in an interfacial region with mixed thermal properties, facilitate phonon conversion across the interface. Using molecular dynamics and Green's function formalisms, it was later demonstrated that an interfacial region with average phonon properties of the solids comprising the interface could bridge the phonon spectra and lead to an increase in phonon transmission and thermal boundary conductance [30–33]. We have also observed that carefully tailored mass impurities between two crystalline solids can increase interfacial transport via the vibrations of the mass impurities [34,35]. Taken together, the theories and simulations indicate that under certain conditions, a "more disordered" interface could have a higher thermal boundary conductance (lower resistance) than a "less disordered, more perfect" interface.

Despite these predictions and computational works, to the best of our knowledge, an increase in any form of disorder has not been experimentally observed to lead to an increase in thermal boundary conductance [1]. Although previous works have demonstrated an increase in thermal boundary conductance through the addition of molecules or functional groups [10,36,37], these works were focused on

*Current address: Seagate Technology, Bloomington, Minnesota 55435, USA.

†phopkins@virginia.edu

increasing interfacial bonding to increase the thermal boundary conductance. For example, we have shown that the thermal conductance across an Al/graphene interface functionalized with oxygen increases compared to a nonfunctionalized interface [10]. Although the functional groups on the graphene led to an increase in disorder on the graphene surface, the increased bond strength between the Al and graphene increased the heat flow. However, this phenomena is fundamentally different than the disorder-induced increase in thermal boundary conductance reported in previous simulations [30–35]. The phonon physics observed in these computational works rely on disorder or additional materials at an otherwise well-bonded interface creating vibrational modes that "bridge" the phonon spectra between two solids; this is in line with the original assertions by Huberman and Overhauser [27] regarding "joint modes" around an interface. Currently, no experimental observations exist that directly support the computational result that the thermal boundary conductance between two well-bonded solids can increase with an increase in interfacial disorder.

In this work, we experimentally demonstrate an increase in the thermal boundary conductance (h_K) across a hydrogen-ion (proton) treated aluminum/native oxide/silicon interface in which the proton irradiation modifies the native oxide silicon surface prior to aluminum evaporation (note, in the samples in which we did not attempt to remove the native oxide, the value for h_K that we report is inversely related to the thermal resistance from the Al film to the Si substrate, which includes the resistance of the Al/native oxide interface, the resistance of the native oxide, and the resistance of the native oxide/Si interface). The ion beam mixing of the native oxide and silicon leads to oxygen and other point defects recoiling into a near-surface region in the silicon, and spatially grades the native oxide into the silicon substrate. This spatial gradation of the silicon native oxide into the silicon changes vibrational characteristics at the surface of the native oxide/silicon substrate, leading to an increase in thermal boundary conductance across the Al/native oxide/Si interfaces. We support this observation with picosecond acoustic analyses, which demonstrates that the ion irradiation shifts the acoustic impedance of the native oxide/silicon surface closer to that of aluminum. We have extensively studied Al/Si interfaces in our previous publications [20,22,38], so the traditional response of a decrease in thermal transport across this interface with roughness and amorphous native oxide layers has been well characterized. Thus, we are able to pinpoint the origin of the increase in the thermal boundary conductance across the Al/native oxide/Si interface as the modification of the native oxide layer into the silicon which manipulates the acoustic impedance of the native oxide/silicon surface.

II. EXPERIMENTAL DETAILS

A. Sample preparation

Prior to Al film deposition, 500-μm-thick [100] silicon substrates were subjected to various surface treatments. We leave one type of sample uncleaned, one series was alcohol cleaned (acetone, isopropyl alcohol, and methanol), and two series of substrates were alcohol cleaned and then subjected to a plasma clean (30 min or 60 min exposures of a 25%/75% O_2/Ar mixture flown at 25 cfm at forward and reverse powers of 57 and 28 W, respectively). These four samples constitute our "nonirradiated" sample set. To create various ion-irradiated Al/Si interfaces, we expose samples to varying levels of proton irradiation followed by either no cleaning, an alcohol clean, or an alcohol clean and then a plasma clean (30 min or 60 min exposures). The proton implantation was performed using a 350 kV HVEE implanter. The ion irradiation was scanned over a masked region on the silicon samples and the suppressed current was directly measured from the sample. We irradiate the silicon samples with 200 keV protons leading to a projected range of 1.84 μm and 134.7 nm of longitudinal straggle determined via SRIM tables [39]. We subjected the silicon to varying doses of protons: 10^{14}, 10^{15}, and 10^{16} protons cm^{-2}. After surface treatment, the Al/Si interfaces were prepared by evaporating nominally 90 nm of Al onto the silicon substrates. Among the various ion irradiation conditions and cleaning procedures, we study 16 different types of Al/Si interfaces. Note that for all 16 of these samples, we made no effort to chemically remove the native oxide on the silicon prior to Al deposition. Additionally, two samples were prepared in which the oxide was removed prior to Al deposition as is discussed in the latter part of this paper.

B. Time-domain thermoreflectance measurements

We measure the thermal boundary conductance at room temperature and ambient conditions with time-domain thermoreflectance (TDTR) [40–43], a pump-probe technique that utilizes short laser pulses to monitor the temperature decay as a function of time on the surface of a metal film. This temporal temperature decay is related to the thermal boundary conductance across the Al/Si interface and the thermal conductivity in the silicon. The analysis is detailed extensively elsewhere [41–43]. Due to the high thermal conductivity of Si, we are able to simultaneously determine both the thermal conductivity of the proton-irradiated Si and the thermal boundary conductance across the Al/Si interface ensuring that our reported values of h_K are not affected by the change in the thermal conductivity of the Si via the proton irradiation. For our measurements, we use pump and probe $1/e^2$ radii of 25 and 10.5 μm, respectively, and a pump-modulation frequency of 11.39 MHz. These experimental parameters not only ensure primarily one-dimensional, cross-plane conduction during our TDTR measurements [42,43], but also establish a thermal penetration depth that is less than the end of range of the irradiated ions [23]. This simplifies our analysis as we only need to consider the substrate as the ion-irradiated silicon and not as a layered system with an ion-implanted layer, a highly defected end of range, and a semi-infinite, unaffected silicon substrate.

Results for the thermal boundary conductance as a function of ion dose are shown in Fig. 1. The sample that is neither cleaned nor irradiated is labeled "as-received." Any surface cleaning increases the thermal boundary conductance by nearly a factor of 2, indicating the importance of cleaning the substrate surfaces to ensure contamination from handling and packaging does not affect h_K. Our values for the nonirradiated, cleaned interfaces agree well with previous measurements

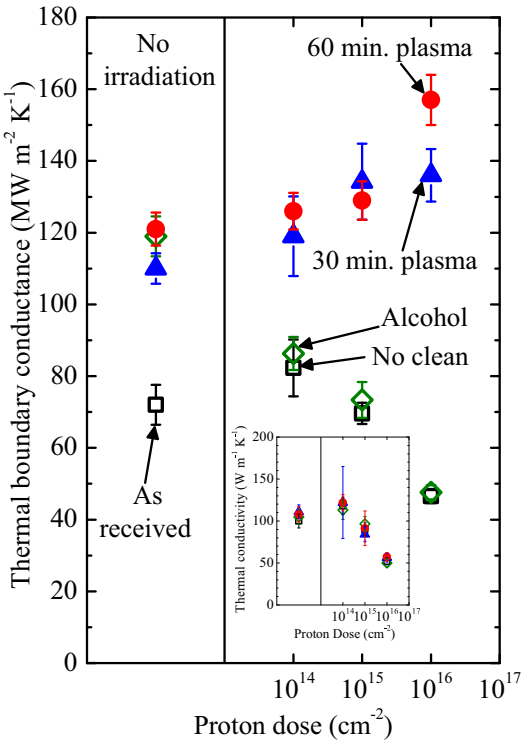

FIG. 1. (Color online) Thermal boundary conductance as a function of proton dose for the various Al/Si interfaces that are examined in this work. The surface treatments are indicated in the figure (no cleaning: open squares, alcohol clean: open diamonds, alcohol clean followed by 30 min plasma clean: filled triangles, alcohol clean followed by 60 min plasma clean: filled circles). In the nonirradiated samples, the factor of nearly 2 increase in h_K when the substrate is cleaned indicates the importance of cleaning as-received wafers to remove contaminants that can affect h_K. The decrease in h_K observed in the ion-irradiated samples that were not subjected to plasma cleaning is due to a build up of carbon contamination on the silicon surface [23,24]. When the carbonaceous layer is removed via plasma cleaning, an increase in h_K is observed. We attribute this increase to ion beam mixing of the native oxide layer with the silicon, which is discussed in detail in the text. The inset shows the measured thermal conductivities of the various silicon substrates as a function of ion dose.

of Al/Si h_K when the Si contains a native oxide layer on the surface and is alcohol cleaned [22]. The decrease in h_K observed in the ion-irradiated samples that were not subjected to plasma cleaning is suspected to be due to a build up of hydrocarbons on the silicon surface resulting from the ion irradiation [23,24]. We confirm the presence of this carbonaceous layer, and its increase with ion dose, with Raman spectroscopy and cross-sectional transmission electron microscopy (TEM) [24]. Plasma cleaning removes the carbon contamination from the Si surface. Interestingly, these cleaned samples show an increase in h_K with an increase in proton dose. To understand the structure and composition of our interfaces, and to gain more insight into the origin of this increase in h_K with proton dose, we analyze our samples using TEM and picosecond acoustics, discussed in the following two sections.

The inset of Fig. 1 shows the measured thermal conductivities of the silicon substrates as a function of ion dose. In general, an increase in ion dose decreases the thermal conductivity of the silicon region that we probe with TDTR. In the highest proton dose, we observe a reduction in thermal conductivity to 50% of the control regardless of the surface cleaning procedure. Note, as previously mentioned, due to our pump modulation frequency, our measurements are sensitive to the volume of silicon defined from the interface to some depth before the end of range of the protons. Therefore, proton irradiation can lead to a decrease in the thermal conductivity of silicon in the volume between the surface and end of range, even though the majority of the structural damage occurs at the end of range. In addition, we do not observe any dependency of the measured thermal conductivity for the different interface conditions at any given proton dose. This suggests that the increase in thermal boundary conductance as a function of proton dose is due to a modification near the interface, and not due to thermal conduction mechanisms in the bulk of the silicon substrate. This also supports the fact that our measured increase in the thermal boundary conductance is intrinsic of the ion irradiation and is not a by-product of the interface leading to nonequilibrium coupling in our measurements [44]. We readdress this concept in Sec. III D.

C. TEM structural and chemical analysis

Cross-section specimens were prepared by an *ex situ* focused-ion-beam (FIB) lift-out technique with a 5 kV final FIB polish. Imaging was conducted by high-angle annular dark field (HAADF) scanning transmission electron microscopy (STEM) using a probe corrected FEI Titan 80–200 and 80–300 instruments, operated at 200 and 300 keV, respectively. The FEI Titan 80–200 instrument is equipped with a SuperX 4-SDD windowless energy dispersive x-ray spectrometer detector array, which was used for composition mapping and analysis. Our STEM measurements identified a distinct interfacial layer between the aluminum film and silicon substrates in all of the analyzed specimens. Figure 2(a) shows examples taken from the (i) nonirradiated alcohol cleaned, (ii) irradiated alcohol cleaned, and (iii) irradiated plasma cleaned samples. In these HAADF-STEM images, the interfacial material shows up as a layer of darker contrast between the Si and Al. In some specimens, we found some localized contamination of the Al from the Ga^+ beam used in the FIB cross-section preparation [bright line of contrast in Fig. 2(a) (ii)].

The interfacial layer thickness, and its variation with irradiation dose, depends sensitively on cleaning conditions. As shown in Fig. 2(b), the layer thickness increases continuously with dose for the specimens cleaned solely with solvent, starting at an initial thickness of 2.2 nm for the unirradiated sample to a thickness of 5.8 nm for the sample irradiated with a dose of 10^{16} cm^{-2}. We attribute this increase in thickness to the hydrocarbon buildup previously discussed [24]. In contrast, for the plasma cleaned samples, the layer thickness remained constant across the full range of doses considered, although the layer thickness was increased with plasma treatment time (30 min: 2.7 nm; 60 min: 3.2 nm). We note that these values for layer thicknesses are in line with typical native oxide layer thicknesses on silicon [22]; in addition, the increase that we observe in our measured h_K does not correlate to any trend in the interfacial layer thickness, which is discussed in more

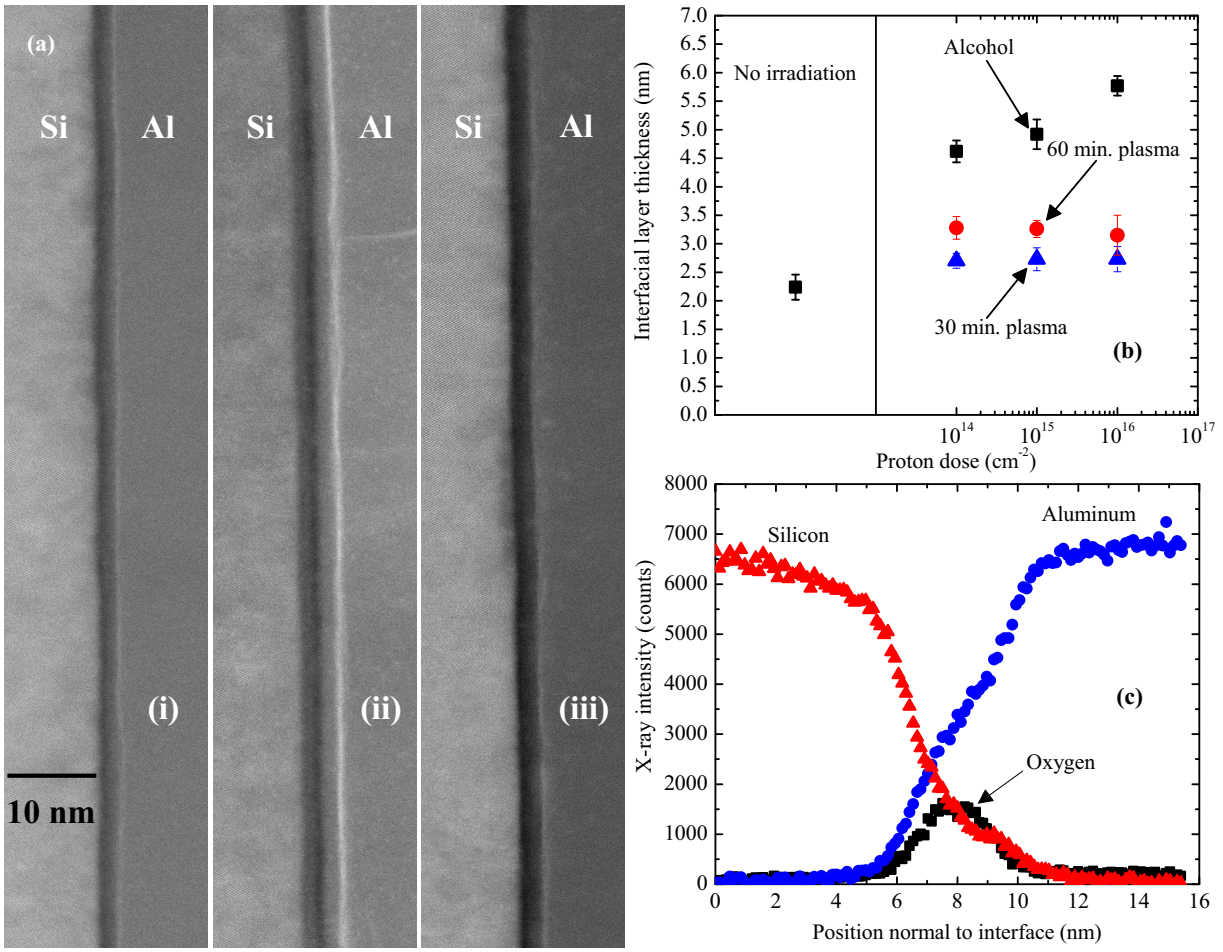

FIG. 2. (Color online) (a) HAADF-STEM images of the interfacial layer between the Al and Si for the (i) nonirradiated alcohol cleaned, (ii) irradiated with 10^{14} protons cm^{-2} and alcohol cleaned, and (iii) irradiated with 10^{14} protons cm^{-2} and plasma cleaned samples. (b) The thicknesses of the interfacial layers, as measured from our TEM analysis, depends on the ion dose when a plasma clean is not used. This is consistent with our observation of carbon contamination building up at the interface with ion dose. When the samples are subjected to a plasma clean post-irradiation, no dose dependence is observed in the interfacial layer thicknesses. (c) Representative EDS profile that shows an enrichment in oxygen at the interfacial layer. This data set was taken on the sample that was irradiated with 10^{14} protons cm^{-2} and plasma cleaned. The onset of the oxygen signal also coincides with the onset of the aluminum signal, indicating the formation of an aluminum-oxide-rich layer from interaction of the Al with the SiO_2 native oxide on the surface of the silicon substrate.

detail later. Furthermore, we do not observe any signatures of crystallization of the native oxide, which implies that our ion irradiation conditions leave the native oxide layer amorphous; this is not surprising given that typical irradiation conditions to crystallize amorphous SiO_2 are at least three orders of magnitude higher doses than those implemented in our current work [45].

We further investigated the composition of the interlayers using energy dispersive x-ray spectroscopy (EDS). As illustrated in the representative EDS profile shown in Fig. 2(c), the interfacial layer is enriched in oxygen. The onset of the oxygen signal also coincides with the onset of the aluminum signal, suggesting the formation of an aluminum-oxide-rich layer from interaction of the Al with the SiO_2 on the surface of the silicon substrate. This signature is observed in all of the samples, even the nonirradiated controls, suggesting that at Al/Si interfaces, the native oxide layer separating the Al and Si is more Al rich than Si rich.

D. Picosecond acoustics

To further characterize these irradiated interfaces, we analyze the picosecond acoustic data from our TDTR measurements [46,47]. During the first few tens of picoseconds of the TDTR response of the thin Al film, the changes in thermoreflectance due to a reflection of a laser-induced strain wave off of the Al/Si interface allow for acoustic properties of the interface to be characterized. These properties are proportional to the temporal response of the in-phase amplitude [48]. Picosecond acoustic analyses have been previously applied to interfaces to identify acoustic impedance changes in thin interfacial layers [49], changes in interfacial bonding [36,50], ion-induced modification of the interfacial bond [48], and varying interfacial roughness at interfaces [8]. Therefore, this represents a suitable tool to gain insight into how the proton irradiation is manipulating the native oxide/near-surface silicon, which can be semiquantitatively related to the thermal results.

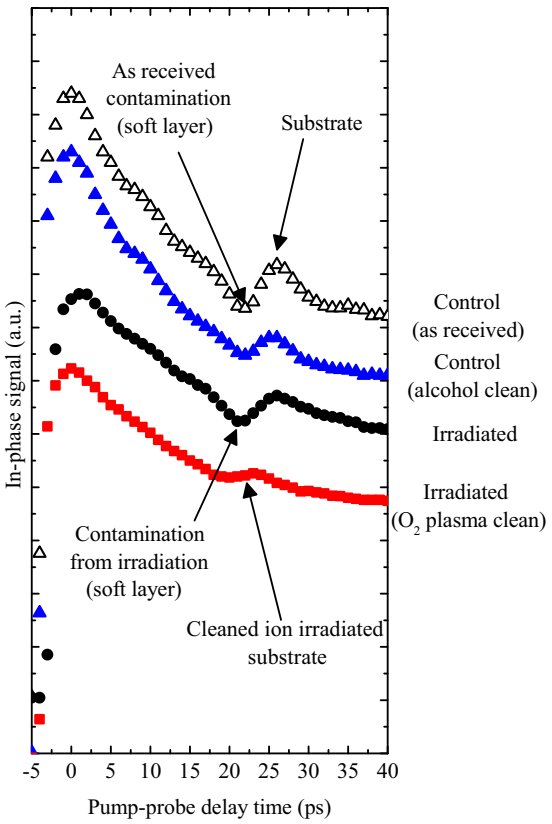

FIG. 3. (Color online) TDTR data focused on the region of the data sets from which picosecond acoustics are monitored to lend insight into the interfacial quality and compositional changes from the different surface treatments (offset for clarity). At the Al/Si interface, a decrease (dip) then increase (hump) is expected due to a strain reflection from the Al off of the native oxide layer and then off of the Si substrate. A dip corresponds to an acoustically softer layer than the Al, originating from either the native oxide, the contamination on the as-received sample (open triangles), or the carbon buildup from the irradiation process (filled circles). Note that this negative trough is diminished with an alcohol clean on the as-received sample (filled triangles), but still observable consistent with the presence of a native oxide. At the plasma cleaned and irradiated interface (filled squares), the amplitude of the strain wave reflection is diminished, which we attribute to a smearing of the native oxide layer and an acoustic impedance of the mixing layer that is closer to that of Al and Si.

As an example, picosecond acoustic data on four different Al/Si samples are shown in Fig. 3. These data consist of an as-received sample with no further cleaning prior to Al evaporation, a sample that has been alcohol cleaned prior to Al evaporation, and ion-irradiated samples (10^{16} protons cm^{-2}) with and without plasma cleaning prior to Al evaporation. Interpretation of the picosecond acoustic data is based on the acoustic impedances of the materials comprising the interfacial region. Larger differences in acoustic impedances lead to stronger amplitudes of the reflected strain wave, and subsequently large "dips" and "humps" in the TDTR signal. As detailed previously [49,51], if a strain wave in the metal film is reflected off of the interface of a material with a higher acoustic impedance than the film, the strain wave will experience a null phase shift and the reflected wave will increase the TDTR signal (i.e., "hump"); however, if the material at the interface has a lower acoustic impedance than that of the film, the wave will undergo a π phase shift and will appear as a "dip" in the TDTR data. Therefore, for a pristine Al/Si interface, we expect a hump in our data since the acoustic impedance of Al is smaller than that of Si. We observe this hump in the as-received data shown in Fig. 3, although we also observe a dip before the hump. We attribute this dip to both carbon contaminants that were not removed prior to metallization and an oxide layer between the Al and Si (originating from the native oxide layer on the Si substrates). In the data in which we clean the substrates with alcohol prior to metallization, we observe a less pronounced negative trough which is indicative of the reflection off of the interfacial oxide layer between the Al and Si alone since much of the "as-received" contaminants were removed via the alcohol clean. We observe the same response in the samples that we plasma treat prior to metallization as we do in the alcohol cleaned samples.

This same analysis can be used to interpret the ion-irradiated data (samples subjected to 10^{16} protons cm^{-2} shown in Fig. 3). The previously discussed carbonaceous layer that forms during ion irradiation results in a strong dip due to the drastically lower acoustic impedance of this layer than the Al film [49]. Removing the carbon layer with a 60 min plasma treatment results in a significant reduction of the picosecond acoustic response. This is not observed at the "contaminant-free" Al/Si interface with an oxide layer ["control (alcohol clean)"]. This implies that the acoustic impedance of the surface of the ion-irradiated samples changes due to the irradiation process, which we discuss in more detail below. We note that since both the alcohol and plasma cleaned samples give the same acoustic response for the nonirradiated samples, we attribute the smaller acoustic response of the plasma cleaned and ion-irradiated samples to an effect of the ion irradiation and not to the surface treatments or to cleaning performed post-irradiation.

III. DISCUSSION

With the above structural and acoustic analyses of our interfaces, we now seek to answer the question: What is the underlying mechanism that is causing an increase in thermal boundary conductance with an increase in ion dose? To address this question, we therefore discuss the results presented in Fig. 1 in the context of the mechanisms identified in the prior computational works, that is, an increase in thermal boundary conductance due to (i) roughness, (ii) a distinct thin film of a different material or mixture, or (iii) a structurally disordered, compositionally graded region with defects.

A. Roughness

Our previous computational work has suggested that a weakly bonded interface with large features of interfacial roughness could increase the incident surface area for the phonon flux, thereby increasing h_K [35]. We do not expect Al to weakly bond to a SiO_2 native oxide layer since we have confirmed that the oxide layer is more Al than Si rich, as previously discussed. Our samples do in fact show a very slight

increase in rms roughness due to the irradiation as measured with atomic force microscopy over the same minimum area of 20 μm × 20 μm. However, the differences in rms roughnesses among the samples is ∼1 nm, with the roughest samples having a maximum rms roughness of ∼1.5 nm. Our previous extensive studies on Al/Si interfaces have shown that an increase in roughness from ∼0.1–5 nm will only impede phonon transport and decrease h_K [20,22,38]. This confirms that our observed increase in h_K is not due to roughness or geometric spatial variability.

B. Thin interfacial film with average properties

Several previous investigations have suggested that a crystalline thin film with average phonon properties of the solids comprising the interface can increase h_K as compared to a perfectly abrupt interface. This is due to gradation of the vibrational density of states that can create a "phonon bridge" that could exist, say, if an alloyed region is inserted between two crystalline solids [30–33]. In our study, the only modification that we impose to our samples is ion irradiation, and since Al and Si are not soluble at room temperature, the creation of some Al-Si alloy is highly improbable. Direct mixing of Al and Si is also improbable due to the presence of the oxide layer between the Al and Si and the fact that ion irradiation was performed prior to Al evaporation on the silicon. The possibility exists that the oxide layer between Al and Si could be serving as a vibrational bridge, since, as seen from our EDS analysis in Fig. 2(c), the oxide layer is Al rich and varying in. However, our compositional analysis with EDS shows no conclusive trend of compositional grading with respect to ion irradiation dose. Thus, it is unlikely that compositional bridging of the Al with the Si through the oxide layer is driving the trends in conductance.

To gain more insight into this concept, we prepared 60 min plasma clean samples with no irradiation and a 10^{16} proton cm^{-2} dose, then used a buffered-oxide etch to remove the oxide layer prior to Al evaporation. The nonirradiated samples have an average thermal boundary conductance of 352 ± 27 MW m^{-2} K^{-1}, consistent with previous measurements of a smooth Al/Si interface with the native oxide layer removed [52]. The irradiated samples' thermal boundary conductances with no oxide exhibit a slight increase in h_K, yielding $h_K = 411 \pm 38$ MW m^{-2} K^{-1}. We note that the difference in resistances ($\Delta R_{\text{no-oxide}} = 1/h_{K,\text{no-irrad}} - 1/h_{K,\text{irrad}}$) is roughly an order of magnitude lower in this case than in the case when we did not remove the native oxide. In other words, $\Delta R_{\text{oxide}} \gg \Delta R_{\text{no-oxide}}$, where, as previously stated, the ΔR refers to change in resistance between the no-irradiation and max-irradiation (10^{16} protons cm^{-2}) conditions. This implies that the majority of the increase in conductance (decrease in resistance) due to proton irradiation observed in Fig. 1 is due to modification of the native oxide layer on silicon. As we have previously concluded that the formation and ion-induced dependency of an Al/Si/oxide mixed film is unlikely, we hypothesize that the proton irradiation of the native oxide/silicon surface is ion mixing the SiO_2 and Si, which leads to a relative increase in h_K. We discuss this in more detail in the following section.

Before discussing our hypothesis that the ion-induced modification of the SiO_2 native oxide on the Si increases the thermal boundary conductance, we cannot ignore the increase in h_K due to irradiation that we observe when the oxide is removed. Upon exposure to proton irradiation, the potential exists for the protons to collide with atoms in the native oxide layer, with a finite probability that oxygen and silicon atoms will recoil at some depth underneath the silicon surface leading to point defects. We conduct TRIM simulations [39] to gain insight into this hypothesis. From these simulations, we estimate that for our irradiation conditions, oxygen impurities can span from 10 parts per billion to 1.0 part per million (ppm) within 2.2 nm of the silicon surface, with 1.0 ppm estimated for the 10^{16} proton cm^{-2} dose. We find that the oxygen impurities (forming Si-O-Si vibrating impurities) can be isolated from each other (i.e., dispersed) in the subsurface silicon region. In addition to oxygen defects, it is important to note that this near-surface region of silicon will also have an increase in silicon point defects including vacancies and self-interstitials, and a higher probability of electron-hole pairs. We therefore attribute the increase in thermal boundary conductance upon proton irradiation in the no-oxide samples (decrease in $\Delta R_{\text{no-oxide}}$) to these aforementioned defects. Although this mechanism of conductance enhancement is not as large as at the mechanism contributing to the increase in h_K across the Al/native oxide/Si interface, it provides experimental evidence supporting our previous molecular dynamics (MD) simulations showing that defects can increase conductance [34].

C. "Vibrational bridging" with compositionally graded, defected regions

The previously discussed "vibrational bridge" effect relies on a distinct, abrupt thin region at the interface that possesses vibrational properties that would effectively "fill in the vibrational gaps" between material 1 (Al) and material 2 (Si). However, our previous computational and theoretical works have suggested another mechanism in which "disorder" can enhance h_K via mass defects [34,53]. The defects can shift the local vibrational density of states around the interface leading to a smooth transition of the vibrational spectra and a subsequently enhanced transmission across the interfacial region. This is similar to the phenomena discussed in Sec. III B above, considering a disordered and spatially diffusive region instead of a crystalline and spatially distinct region with a unique phonon spectrum. Unlike our discussion in Sec. III B above, we explore the possibility of a vibrational bridge occurring from modifications of the SiO_2 native oxide/silicon interface from the proton irradiation.

To test this hypothesis, we refer to our previous discussion regarding picosecond acoustics. Figure 3 demonstrates that the acoustic reflection at the interface of the Al and ion-irradiated silicon is modified due to the irradiation processes. In addition, our TRIM simulations discussed above confirm that the ion conditions lead to a finite probability of oxygen defects near the surface of the silicon. The resulting Si-O bond that will form in the sub-Si surface region will lead to Si-O-Si impurity sites with local masses greater than the unaltered silicon lattice. The increased mass of these impurities may shift the vibrational spectra in the defected region due to the lower frequency

vibrations of the heavier impurities as compared to silicon. As we show in our previous simulations [34], this can modify the density of states near the interface, shifting vibrations to lower frequencies that could "bridge" the phonon spectra of the Al film and the Si substrate. From phonon matching theory [2], this would lead to increased overlap in the vibrational spectrum in the Al and the near-interfacial region of the Si causing an increase in phonon transmission (note, we have also observed computationally that better spectral overlap of the acoustic phonon branches leads to an increase in h_K) [54].

This explanation is difficult to prove with our structural analysis since individual oxygen and silicon point defects are beyond the resolution of any TEM technique currently available. However, an acoustic impedance analysis with corresponding picosecond acoustic data supports this theory. Figure 3 shows that the picosecond acoustic amplitude decreases when silicon is subjected to our ion irradiation procedure. The native oxide-based defects that recoil into the silicon would therefore shift the acoustic impedance of the surface region of silicon closer to the native oxide, which would lead to a larger acoustic transmission (smaller amplitude of reflection). In other words, the defected interfacial regions of acoustic impedance Z_i will enhance h_K by spatially grading the vibrations between two materials if $Z_A \leqslant Z_i \leqslant Z_B$, where Z_A and Z_B represent the acoustic impedances of the materials comprising the interface; this is consistent with our previous computational results [34].

For our samples, the increase in the oxygen and other point defects in the silicon effectively causes the abrupt native oxide layer to mix with the silicon substrate, or become less abrupt, prior to Al evaporation. This results in various Al/oxide/Si interfaces in which the oxide is compositionally graded into the silicon depending on the ion dose (note, as previously mentioned, our proton irradiation procedure only modifies the interface between the native oxide and the silicon substrate). This is not surprising, as previous works have demonstrated that irradiation will modify the native oxide layer on silicon [55]. In the hypothetical case of a compositionally abrupt Al/oxide/Si interface, the acoustic impedance of the oxide is less than both that of Al and Si ($Z_{Si} = 1.9 \times 10^6$ g cm^{-2} s^{-1} > $Z_{Al} = 1.7 \times 10^6$ g cm^{-2} s^{-1} > $Z_{SiO_2} = 1.3 \times 10^6$ g cm^{-2} s^{-1}, where $Z = \rho v$, where ρ is the mass density and v is the speed of sound). However, as the compositional abruptness of the oxide layer decreases, the average acoustic impedance in the near-surface region of the silicon will decrease to values more similar to the Al. This results in an increase in thermal boundary conductance, consistent with our measured data in Fig. 1 and our recent MD simulations [34]. This also explains our data in which we removed the native oxide layer before Al evaporation, since the implanted defects in the Si substrate will lower the acoustic impedance of the silicon and increase the number of low-frequency vibrations that overlap with the Al modes.

Figure 4 shows the picosecond acoustic analysis of representative samples that illustrate the effects of irradiation and cleaning processes on the acoustic impedance of the interfacial region. Figure 4(a) shows the residuals of representative data calculated by subtracting the thermal decay signature from our TDTR data. All these data are taken from TDTR measurements on samples that have been plasma cleaned to avoid the picosecond acoustic signature from the carbon layer. The amplitudes of the residuals clearly decrease as the proton dose increases. Figure 4(b) quantifies the peak-to-peak amplitudes of the data shown in Fig. 4(a) as a function of proton dose, supporting our contention that an increase in proton dose, which increases thermal boundary conductance, is correlated to an increase in the ion beam mixing of the native oxide layer and silicon substrate. Those near-surface defects create low-frequency vibrations in the interfacial region of silicon, leading to a decrease in the acoustic impedance and the decrease in the amplitude of the picosecond acoustic response. Here we have observed a correlation between an increase in thermal boundary conductance with an increase in near-interface defect density.

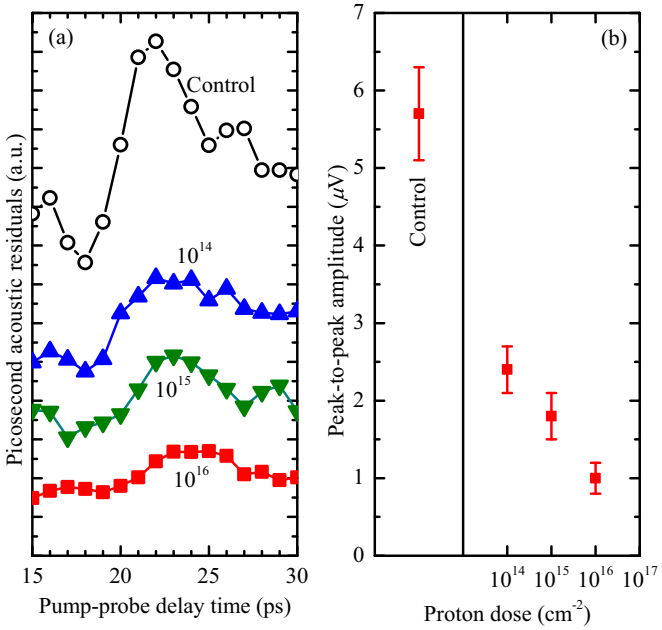

FIG. 4. (Color online) (a) Picosecond acoustic residuals as a function of pump-probe delay time from our TDTR data on the plasma cleaned samples subjected to various proton doses. The various proton doses are indicated in the figure; the control sample was not subjected to any ion irradiation. An increase in proton dose leads to a decrease in the reflected amplitude of the acoustic wave off of the Al/oxide/Si interface. This indicates a shift in the low-frequency vibrational properties of the silicon near the surface. (b) Peak-to-peak amplitude of the picosecond acoustic residuals shown in (a) as a function of ion dose.

D. Additional considerations

Our experimental measurements of thermal boundary conductance and their correlation to our picosecond acoustic analysis suggest that the proton irradiation of the SiO_2 native oxide/Si surface increases the acoustic impedance of the interfacial region between the Al film and Si substrate. We attribute the subsequent increase in conductance, which correlates to the changing acoustic impedance, to spatial gradation of the native oxide and subsequent defect creation in the silicon. However, we cannot preclude the possibility that additional by-products from our ion irradiation and cleaning procedures

or experimental factors from our TDTR measurements could be affecting our reported results in Fig. 1.

As previously discussed, the native oxide layer between Al and Si can pose a non-negligible resistance to the thermal boundary conductance from the Al to the Si [20,22]. Our previous work in Refs. [20] and [22] suggest that, to a first approximation, the difference between the resistance measured across an Al/native oxide/Si interface and that across an Al/Si interface (with the native oxide removed) can be approximated as the thermal resistance of the native oxide, given by $d_{\text{oxide}}/\kappa_{\text{oxide}}$, where d_{oxide} is the native oxide thickness and κ_{oxide} is the thermal conductivity of the native oxide. Clearly, a change in these properties of the interfacial region could also contribute to our observed increase in h_{K} across the Al/native oxide/Si interface. However, a modification in d_{oxide} or κ_{oxide} that would increase h_{K} in our reported data is unlikely. For example, in Fig. 2(b), we consistently observe that the thickness of the interfacial region does not depend on ion dose of the oxygen plasma cleaned samples. In fact, we find that oxygen plasma cleaning slightly increases the interfacial layer thickness. However, in our control samples, we do not observe a statistically significant, consistent change in h_{K} due to the oxygen cleaning procedure. Therefore, we do not expect the change in native oxide thickness to be the cause of the increase in thermal boundary conductance with proton irradiation.

Another mechanism which might increase h_{K} with proton dose is a decrease in resistance of the interfacial oxide from an increase in intrinsic thermal conductivity of the native oxide region as opposed to our proposed spatial gradation of the oxide region. For example, if the native oxide layer were to increase in density due to the ion irradiation, the thermal conductivity of this amorphous region could also increase [56,57]. This would also increase the acoustic impedance of this region which could explain the picosecond acoustic signatures in Fig. 4. However, as we previously mentioned, we do not expect the ion energies to be high enough to cause a significant change in the amorphous morphology in the native oxide layer prior to Al evaporation [45], so this possibility is unlikely.

Along these lines, an additional possibility is that the change in stoichiometry of the interfacial oxide increases the intrinsic thermal conductivity of the amorphous layer, thereby increasing the measured thermal boundary conductance from the Al to Si. Depending on the density, the thermal conductivity of amorphous Al_2O_3 has been reported to be as high as 1.65 W m^{-1} K^{-1} [58,59], approximately 20% larger than the thermal conductivity of bulk SiO_2 [57]. Although we cannot directly measure the intrinsic thermal conductivity of this thin interfacial oxide, we do not observe any change in spatial composition with increased proton dose within the limits of our four simultaneous EDS detector analysis, suggesting that the increase in h_{K} is not related to spatial stoichiometry of the oxide region. Furthermore, the fact that we still observe an increase in h_{K} with proton dose when removing the oxide prior to Al evaporation (Sec. III B) further supports the case that this vibrational bridge effect is most likely the mechanism causing an increase in h_{K} with proton dose.

Finally, recent works [52,60,61] that have observed both radial and frequency dependence in thermal conductivity measurements of silicon using TDTR or related techniques have theorized that these effects are driven by nonlocal heat conduction around the interface of a metal film and silicon substrate [44]. This nonlocal effect can affect our measurements of both thermal conductivity in the silicon and the measured thermal boundary conductance, as the gradient of energy could be a by-product of our TDTR experimental parameters. Therefore, one could hypothesize that this nonlocal effect could be contributing to the observed trend of an increase in h_{K} with an increase in proton dose. For example, the modification of the interfacial region from the ion irradiation could change the number of phonons being transmitted through the oxide region without being scattered and thus affect the TDTR-derived measurements of h_{K}. To this point, however, as mentioned in Sec. II B, for any given proton dose, we measure the same thermal conductivity of the silicon substrate (within experimental uncertainty), regardless of the cleaning procedure. For the highest dose samples, the measured thermal boundary conductance spans a factor of 3 while the measured thermal conductivities remain constant. If nonlocal effects were driving our observed trends in h_{K} vs proton dose in Fig. 1, we would also expect that this nonlocal phonon transport would lead to different measured temperature gradients in the silicon, and therefore affect the TDTR-derived measurements of thermal conductivity of the silicon. Since we are not able to resolve any clear change in the measured thermal conductivity of silicon, we assert that this nonlocal effect in TDTR measurements is not the underlying reason for the measured increase in h_{K} vs proton dose. This further supports our vibrational bridge mechanism as the cause of the increase in h_{K} with proton dose, as detailed in Sec. III B.

In line with these discussions of nonlocal phonon transport affecting TDTR measurements [44], we point out that our measurements of thermal conductivity of silicon reported in the inset of Fig. 1 are lower than the accepted literature values for the thermal conductivity of bulk silicon (124–156 W m^{-1} K^{-1}) [62–65]. Although we attribute the increasing trends in h_{K} vs proton dose to be due to the vibrational bridge effect and not nonlocal transport (discussed above), we cannot rule out the possibility that the absolute values of our measurements of thermal conductivity could be affected by some aspect of this nonlocal transport during TDTR. This would imply that the near-surface region of the substrate affects the nonlocal phonon transport in the silicon and resulting measurements of thermal conductivity, consistent with previous theory [44]. As we measure the same thermal conductivity regardless of ion dose, yet different thermal boundary conductances based on the post-irradiation surface cleaning (which would not change the ion modified region), this supports both the nonlocal theory and our assertion about the increase in h_{K} with an increase in proton dose being driven by "vibrational bridging."

These realizations may offer insight into variations found in literature regarding measurements of thermal boundary conductance across Al/Si interfaces. In several of our previous works [1,20–23,66], we have measured the thermal boundary conductance across Al/native oxide/Si interfaces with different interfacial properties. In general, the measured values of h_{K} across the various interfaces span from ∼110–200 MW m^{-2} K^{-1}. In this current work, we report thermal boundary conductances from ∼110–120 MW m^{-2} K^{-1} with

silicon thermal conductivities of $\sim$100–110 W m^{-1} K^{-1}. However, in a previous work [23], we measured a thermal boundary conductance of 200 MW m^{-2} K^{-1} and a silicon thermal conductivity of 133 W m^{-1} K^{-1}, in better agreement with the accepted literature values for bulk silicon [62–65]. This implies that the measured thermal conductivity in the silicon substrate could be directly correlated to the resistance at the Al/Si interfacial region, consistent with the nonlocal description of heat transfer near an interface and its effect on TDTR measurements. In the arguments put forth above, we present reasons why we do not believe this is the underlying mechanism causing h_K to increase with proton dose in our current work, although this could be affecting the absolute values reported in this paper. Future work could study this effect in much greater detail by correlating TDTR measurements of thermal conductivity with thermal boundary conductance across solid interfaces with nanoscale "imperfections" [1].

IV. CONCLUSIONS

In summary, we have demonstrated the ability to increase the thermal boundary conductance across aluminum/native oxide/silicon interfaces by proton irradiation of the native oxide/silicon surface. We hypothesize that spatial gradation of atomic masses increases the thermal boundary conductance from the Al film to the Si substrate even though the interfacial region is noncrystalline and defected. The ion mixing creates improved matching of acoustic impedances resulting in an increase in thermal boundary conductance as the spatial extent of compositional and structural disorder increases. Although this result is counterintuitive in terms of the traditional view of phonon-impurity scattering in homogeneous crystals, it is consistent with recent computational studies on the effect of mass impurities around interfaces of two solids by creating a "bridge" of mass and vibrational properties. These results experimentally demonstrate this bridging effect across a well-bonded interface with a physical system.

Our observation of an increase in thermal boundary conductance with proton exposure sets the stage for future studies involving ion irradiation of different species and energies to bidirectionally tune the thermal conductance across solid interfaces. As we have shown with our picosecond acoustic analysis, the acoustic impedance of the near-surface SiO_2/Si region clearly changes with ion irradiation. While our TRIM calculations predict that this mechanism is due to defect formation and recoil of the native oxide atoms into the near-surface silicon region, future studies can explore this result in more detail by considering heavier ions to create more dynamic mobility and recoil of the native oxide atoms along with different degrees of defect formation in the near-surface region. For example, heavier ions could increase the probability of dislocation loops, greater Frenkel pair density, and amorphous regions in the crystalline substrate. This could create an additional variable by which to control thermal boundary conductance across solid interfaces via defect formation. However, to further explore this effect, during ion beam modification of the film, interface, or substrate, care must be taken to isolate the effects of these interfacial impurities formed via ion mixing from the tailored displacement damage.

ACKNOWLEDGMENTS

We appreciate support from the Office of Naval Research Young Investigator Program (Grant No. N00014-13-4-0528), the Army Research Office (Grant No. W911NF-13-1-0378), and the Laboratory Directed Research and Development (LDRD) program at Sandia National Laboratories. Additionally, the authors acknowledge John Bradley for allowing use of the 80-300 Titan S/TEM at Lawrence Livermore National Laboratory. Sandia is a multiprogram laboratory managed and operated by Sandia Corporation, a wholly owned subsidiary of Lockheed Martin Corporation, for the US Department of Energy's National Nuclear Security Administration under Contract No. DE-AC04-94Al85000.

[1] P. E. Hopkins, ISRN Mech. Eng. **2013**, 682586 (2013).
[2] E. T. Swartz and R. O. Pohl, Rev. Mod. Phys. **61**, 605 (1989).
[3] D. G. Cahill, W. K. Ford, K. E. Goodson, G. D. Mahan, A. Majumdar, H. J. Maris, R. Merlin, and S. R. Phillpot, J. Appl. Phys. **93**, 793 (2003).
[4] E. Pop, Nano Res. **3**, 147 (2010).
[5] R. M. Costescu, D. G. Cahill, F. H. Fabreguette, Z. A. Sechrist, and S. M. George, Science **303**, 989 (2004).
[6] C. Chiritescu, D. G. Cahill, N. Nguyen, D. Johnson, A. Bodapati, P. Keblinski, and P. Zschack, Science **315**, 351 (2007).
[7] W.-L. Ong, S. M. Rupich, D. V. Talapin, A. J. H. McGaughey, and J. A. Malen, Nat. Mater. **12**, 410 (2013).
[8] J. C. Duda, P. E. Hopkins, Y. Shen, and M. C. Gupta, Phys. Rev. Lett. **110**, 015902 (2013).
[9] J. Liu, B. Yoon, E. Kuhlmann, M. Tian, J. Zhu, S. M. George, Y.-C. Lee, and R. Yang, Nano Lett. **13**, 5594 (2013).
[10] P. E. Hopkins, M. Baraket, E. V. Barnat, T. E. Beechem, S. P. Kearney, J. C. Duda, J. T. Robinson, and S. G. Walton, Nano Lett. **12**, 590 (2012).
[11] J. C. Duda, P. E. Hopkins, Y. Shen, and M. C. Gupta, Appl. Phys. Lett. **102**, 251912 (2013).
[12] X. Wang, C. D. Liman, N. D. Treat, M. L. Chabinyc, and D. G. Cahill, Phys. Rev. B **88**, 075310 (2013).
[13] A. I. Hochbaum, R. Chen, R. D. Delgado, W. Liang, E. C. Garnett, M. Najarian, A. Majumdar, and P. Yang, Nature (London) **451**, 163 (2008).
[14] A. I. Boukai, Y. Bunimovich, J. Tahir-Kheli, J. K. Yu, W. A. Goddard, and J. R. Heath, Nature (London) **451**, 168 (2008).
[15] R. Cheaito, J. C. Duda, T. E. Beechem, K. Hattar, J. F. Ihlefeld, D. L. Medlin, M. A. Rodriguez, M. J. Campion, E. S. Piekos, and P. E. Hopkins, Phys. Rev. Lett. **109**, 195901 (2012).
[16] P. Chen, N. A. Katcho, J. P. Feser, W. Li, M. Glaser, O. G. Schmidt, D. G. Cahill, N. Mingo, and A. Rastelli, Phys. Rev. Lett. **111**, 115901 (2013).
[17] W. Kim, J. Zide, A. Gossard, D. Klenov, S. Stemmer, A. Shakouri, and A. Majumdar, Phys. Rev. Lett. **96**, 045901 (2006).

[18] D. Li, Y. Wu, R. Fan, P. Yang, and A. Majumdar, Appl. Phys. Lett. **83**, 3186 (2003).
[19] C. W. Chang, D. Okawa, A. Majumdar, and A. Zettl, Science **314**, 1121 (2006).
[20] J. C. Duda and P. E. Hopkins, Appl. Phys. Lett. **100**, 111602 (2012).
[21] P. E. Hopkins, J. C. Duda, C. W. Petz, and J. A. Floro, Phys. Rev. B **84**, 035438 (2011).
[22] P. E. Hopkins, L. M. Phinney, J. R. Serrano, and T. E. Beechem, Phys. Rev. B **82**, 085307 (2010).
[23] P. E. Hopkins, K. Hattar, T. Beechem, J. F. Ihlefeld, D. L. Medlin, and E. S. Piekos, Appl. Phys. Lett. **98**, 231901 (2011).
[24] P. E. Hopkins, K. Hattar, T. Beechem, J. F. Ihlefeld, D. L. Medlin, and E. S. Piekos, Appl. Phys. Lett. **101**, 099903 (2012).
[25] P. E. Hopkins, J. C. Duda, S. P. Clark, C. P. Hains, T. J. Rotter, L. M. Phinney, and G. Balakrishnan, Appl. Phys. Lett. **98**, 161913 (2011).
[26] P. E. Hopkins, P. M. Norris, R. J. Stevens, T. Beechem, and S. Graham, J. Heat Transfer **130**, 062402 (2008).
[27] M. L. Huberman and A. W. Overhauser, Phys. Rev. B **50**, 2865 (1994).
[28] R. J. Stoner, H. J. Maris, T. R. Anthony, and W. F. Banholzer, Phys. Rev. Lett. **68**, 1563 (1992).
[29] R. J. Stoner and H. J. Maris, Phys. Rev. B **48**, 16373 (1993).
[30] R. J. Stevens, L. V. Zhigilei, and P. M. Norris, Int. J. Heat Mass Transfer **50**, 3977 (2007).
[31] Z. Liang and H.-L. Tsai, J. Phys.: Condens. Matter **23**, 495303 (2011).
[32] T. S. English, J. C. Duda, J. L. Smoyer, D. A. Jordan, P. M. Norris, and L. V. Zhigilei, Phys. Rev. B **85**, 035438 (2012).
[33] Z. Tian, K. Esfarjani, and G. Chen, Phys. Rev. B **86**, 235304 (2012).
[34] J. C. Duda, T. S. English, E. S. Piekos, T. E. Beechem, T. W. Kenny, and P. E. Hopkins, J. Appl. Phys. **112**, 073519 (2012).
[35] X. W. Zhou, R. E. Jones, C. J. Kimmer, J. C. Duda, and P. E. Hopkins, Phys. Rev. B **87**, 094303 (2013).
[36] M. D. Losego, M. E. Grady, N. R. Sottos, D. G. Cahill, and P. V. Braun, Nat. Mater. **11**, 502 (2012).
[37] P. J. O'Brien, S. Shenogin, J. Liu, P. K. Chow, D. Laurencin, P. H. Mutin, M. Yamaguchi, P. Keblinski, and G. Ramanath, Nat. Mater. **12**, 118 (2013).
[38] P. E. Hopkins, J. C. Duda, and P. M. Norris, J. Heat Transfer **133**, 062401 (2011).
[39] J. F. Ziegler, Nucl. Instrum. Methods Phys. Res., Sect. B **219-220**, 1027 (2004).
[40] D. G. Cahill, K. E. Goodson, and A. Majumdar, J. Heat Transfer **124**, 223 (2002).
[41] D. G. Cahill, Rev. Sci. Instrum. **75**, 5119 (2004).
[42] A. J. Schmidt, X. Chen, and G. Chen, Rev. Sci. Instrum. **79**, 114902 (2008).
[43] P. E. Hopkins, J. R. Serrano, L. M. Phinney, S. P. Kearney, T. W. Grasser, and C. T. Harris, J. Heat Transfer **132**, 081302 (2010).
[44] R. B. Wilson, J. P. Feser, G. T. Hohensee, and D. G. Cahill, Phys. Rev. B **88**, 144305 (2013).
[45] A. F. Cohen, J. Appl. Phys. **29**, 591 (1958).
[46] C. Thomsen, J. Strait, Z. Vardeny, H. J. Maris, J. Tauc, and J. J. Hauser, Phys. Rev. Lett. **53**, 989 (1984).
[47] C. Thomsen, H. T. Grahn, H. J. Maris, and J. Tauc, Phys. Rev. B **34**, 4129 (1986).
[48] G. Tas, J. J. Loomis, H. J. Maris, A. A. Bailes, and L. E. Seiberling, Appl. Phys. Lett. **72**, 2235 (1998).
[49] G. T. Hohensee, W.-P. Hsieh, M. D. Losego, and D. G. Cahill, Rev. Sci. Instrum. **83**, 114902 (2012).
[50] B. C. Daly, H. J. Maris, K. Imamura, and S. Tamura, Phys. Rev. B **66**, 024301 (2002).
[51] C. Chiritescu, Ph.D. thesis, University of Illinois at Urbana-Champaign, 2010.
[52] A. J. Minnich, J. A. Johnson, A. J. Schmidt, K. Esfarjani, M. S. Dresselhaus, K. A. Nelson, and G. Chen, Phys. Rev. Lett. **107**, 095901 (2011).
[53] T. Beechem and P. E. Hopkins, J. Appl. Phys. **106**, 124301 (2009).
[54] X. W. Zhou, R. E. Jones, J. C. Duda, and P. E. Hopkins, Phys. Chem. Chem. Phys. **15**, 11078 (2013).
[55] H. Dallaporta and A. Cros, Appl. Phys. Lett. **48**, 1357 (1986).
[56] P. E. Hopkins, B. Kaehr, E. S. Piekos, D. Dunphy, and C. J. Brinker, J. Appl. Phys. **111**, 113532 (2012).
[57] R. M. Costescu, A. J. Bullen, G. Matamis, K. E. O'Hara, and D. G. Cahill, Phys. Rev. B **65**, 094205 (2002).
[58] S. M. Lee, D. G. Cahill, and T. H. Allen, Phys. Rev. B **52**, 253 (1995).
[59] C. S. Gorham, J. T. Gaskins, G. N. Parsons, M. D. Losego, and P. E. Hopkins, Appl. Phys. Lett. **104**, 253107 (2014).
[60] T. S. English, L. M. Phinney, P. E. Hopkins, and J. R. Serrano, J. Heat Transfer **135**, 091103 (2013).
[61] K. T. Regner, D. P. Sellan, Z. Su, C. H. Amon, A. J. H. McGaughey, and J. A. Malen, Nat. Commun. **4**, 1640 (2013).
[62] C. Y. Ho, R. W. Powell, and P. E. Liley, J. Phys. Chem. Ref. Data **1**, 279 (1972).
[63] F. Incropera and D. P. DeWitt, *Fundamentals of Heat and Mass Transfer*, 4th ed. (Wiley, New York, 1996).
[64] D. R. Lide, *CRC Handbook for Chemistry and Physics*, 89th ed. (CRC Press/Taylor and Francis, Boca Raton, FL, 2008).
[65] C. J. Glassbrenner and G. A. Slack, Phys. Rev. **134**, A1058 (1964).
[66] P. E. Hopkins, T. E. Beechem, J. C. Duda, K. Hattar, J. F. Ihlefeld, M. A. Rodriguez, and E. S. Piekos, Phys. Rev. B **84**, 125408 (2011).